ACS APPLIED MATERIALS & INTERFACES
Research Article
www.acsami.org

Holistic Method for Evaluating Large Area Transparent Conducting Electrodes

Ritu Gupta and Giridhar U. Kulkarni*

Chemistry and Physics of Materials Unit, DST Unit on Nanoscience, Jawaharlal Nehru Centre for Advanced Scientific Research, Jakkur P.O., Bangalore, India-560064

Supporting Information

ABSTRACT: Nowadays, specifying the quality of a transparent conducting electrode (TCE) using a figure of merit (FoM) is considered nearly mandatory. However, not much attention is paid to the local variations in the FoM itself across the large area of the TCE. This calls for the definition of a local FoM (LFoM), particularly relevant with regard to several new generation TCEs which have been and are being proposed recently. A LFoM based on local measurements of transmission and sheet resistance, pixel by pixel, would be a Herculean task. The present article addresses this central issue by defining a LFoM based on the diffraction efficiency (*DE*) of a calibrated high-resolution transmission grating overlaid with a given TCE. The *DE* value, which critically depends on the periodic nature of the grating material, is shown to be highly sensitive to the various nonuniformities in the TCE overlaid on the grating, with length scales comparable to the grating period. The effectiveness of the so-defined LFoM was demonstrated using a pointer laser and a photodiode in combination with a transmission grating with ∼μm periodicity by taking ITO/glass and ITO/PET as case examples. A metal grating pattern of Cu deposited on seed Pd grating lines was fabricated as an example of new generation TCE and examined for FoM and LFoM, however, without the aid of the external grating. The LFoM based on *DE* presented here should serve as an excellent screening method for both conventional and emerging TCEs.

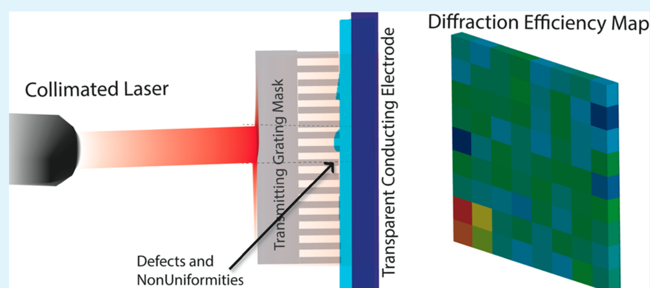

KEYWORDS: *Figure of Merit, transmittance, diffraction efficiency, surface defects, uniformity*

INTRODUCTION

There is intense research pursued worldwide in the field of transparent conducting electrodes (TCEs) because of their inevitable use in various optoelectronic devices such as flat panel displays and solar cells, as well as for low emissivity and defrosting windows, electromagnetic shields, and invisible security circuits.[1,2] Currently used TCEs are mostly indium−tin-oxide (ITO) which exhibits transparency, $T > 90\%$, and sheet resistance, $R_s \approx 10$–$100\ \Omega$/sq at film thicknesses of ∼100 nm.[3] Besides conventional ITO, several new materials have been projected as candidates for TCE, with notable ones being few-layer graphene,[4−10] carbon nanotube network,[11−15] metal nanowire mesh,[16−20] nanocomposites of graphene and carbon nanotubes,[21] and metal nanostructures in polymer.[22]

The quality of a TCE is expressed by its Figure of Merit (FoM). In the literature, there is much discussion on how a FoM can be defined and determined for a given TCE.[23,24] A brief survey is given in Supporting Information Table S1. While T/R_s can serve as a FoM, historically, the definition given by Haacke[25]

$$\phi_{TCE} = (T^{10}/R_s) \tag{1}$$

is used. Usually, the values of FoM as in eq 1 are in the range of 1×10^{-4} -to $4 \times 10^{-3}\ \Omega^{-1}$ for different TCEs. This definition holds good for conventional oxides (TCOs), but the emerging TCEs based on network structure are treated with a different definition since T can acquire a value above 90% and R_s is not proportional to thickness in the percolation regime.[25] FoM expressed as the ratio of DC conductivity and optical conductivity (σ_{DC}/σ_{OP}), is commonly used for film thicknesses less than the wavelength of light.[26] Higher value of σ_{DC}/σ_{OP} corresponds to a material with high optical transmittance and low electrical resistance, with a typical value for ITO being 350–400.[26] According to the industry standard, $T > 90\%$ and $R_s < 100\ \Omega$/sq is required, which results in σ_{DC}/σ_{OP} ratio greater than 35. Recently, a comparison between the emerging nanostructured TCEs and the conventional TCOs has been made in the light of FoM definition to highlight some important differences which have been somewhat ignored in the rush of developing new TCEs.[27]

Although FOMs by and large address the requirements of a TCE, one of the pertinent problems is not given enough attention in the literature. This is associated with producing large-area TCEs with uniformity in transmittance and sheet resistance, or in other words, uniformity in FoM. This may not be much of a problem in the case of thin-film TCEs such as ITO films, where uniformity in thickness can be well monitored

Received: October 9, 2012
Accepted: December 30, 2012
Published: December 31, 2012

 © 2012 American Chemical Society

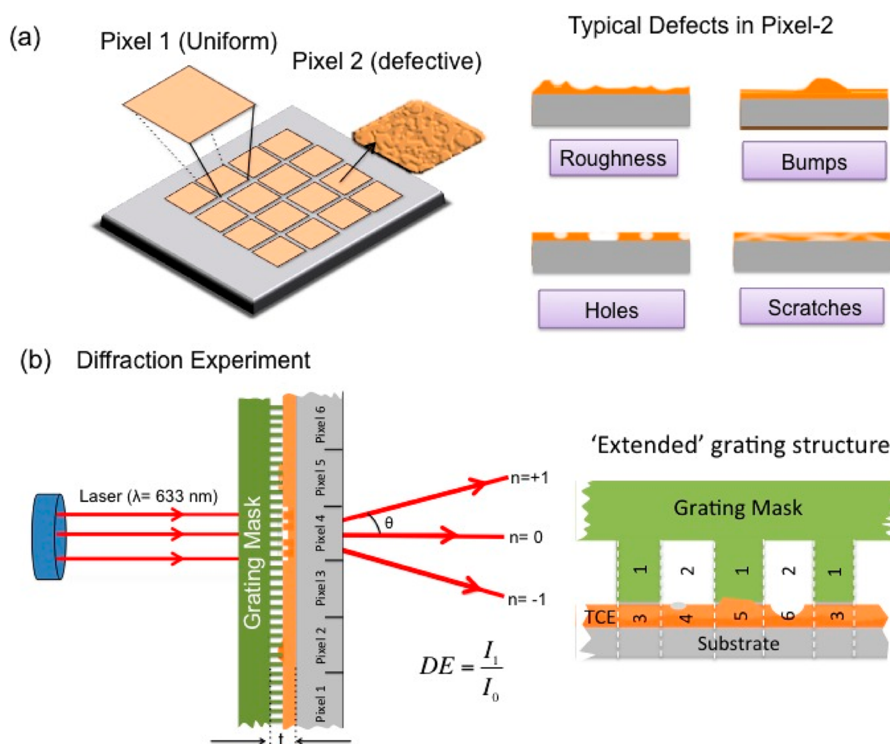

Figure 1. (a) A pixelated TCE film exhibiting possible non-uniformities; pixel 1 is smooth and contains uniformly deposited TC material, while pixel 2 represents a defective region. The types of defects typically encountered are depicted on the right. If absorption is taken to indicate the uniformity in a pixel, it may turn out to be a poor representation in the case of a pixel hosting different defects; the holes increase transmission of light while bumps may decrease it. These deviations compared to absorption from a smooth region may cancel each other such that overall absorption of pixel 2 may be similar to that in pixel 1 (smooth region). (b) The pixelated TCE under examination, overlaid with a transmitting grating in an optical diffraction experiment with the light source illuminating a pixel. The grating period is typically one tenth of the pixel dimension. This is essentially an "extended" grating structure as shown magnified on the right. The numbers marked, 1−6, represent (η and κ) pairs from the different parts of the extended grating, relevant in DE expression (see discussion below). The diffraction efficiency (DE) is used here to evaluate the uniformity of the pixel, as it is more sensitive than simple absorption measurement. Essentially, this is experimental Fourier analysis of the pixel region for examining the non-uniformities that affect transmission

during deposition. On the other hand, emerging TCEs such as CNT or metal nanowire networks are based on nudity with respect to the incident light at different length scales, instead of uniform coverage. In such cases, ensuring uniformity of FoM becomes more involved. Kaskela et al.[28] examined the uniformity (see Figure S10 of ref 28) by measuring transmittance and sheet resistance at 9 arbitrary locations over a large area. The Coleman group[29] studied the uniformity of the CNTs and CNT−graphene composite films by calculating the standard deviation in the absorbance using the transmission map of the entire film recorded using a commercial scanner. Similarly, the uniformity in conductivity can be monitored by current mapping using a conductive-AFM, although the process is relatively more tedious and therefore impractical.[30] There are, however, a few recent examples in the literature of resistance mapping of large areas of CNT[31] and graphene oxide thin films.[32,33]

In this article, we have addressed the issue of nonuniformity and surface defects and presented a new approach to specify the uniformity of a TCE. In this method, the diffraction efficiency (DE) of a standard transmission grating attached to a TCE under examination is measured at every pixel and any deviation in its value indicates a defect in the TCE. The method is highly sensitive in detecting defects in thickness and composition as well as other minute nonuniformities, which are typically beyond visual inspection. The absorption measurements in local regions may exhibit only small differences and even be quite deceptive (see Figure 1). In other words, the DE value at a pixel serves as its local FoM or LFoM. Among the new-generation TCEs, many are lithographically defined periodic nanostructures[34] and in such cases, the method becomes more straightforward in that the diffraction measurements can be performed directly on the TCE itself without the aid of an external grating. An example of this kind is also presented. While the above method is clearly applicable to the diverse range of new-generation TCEs, it does not prevent one using it to examine simply the defects on a nonconducting sheet or for that matter, any optical element.

As an example to deal with, we chose metal grating patterns with line widths in μms (μ-MGPs). Previously, Tvingstedt et al.[35] fabricated micrometer line gratings and Kang et al.[36,37] produced Ag, Au, and Cu line gratings with submicrometer periodicity over large areas to use as TCE. Using Pd as seed layer, we have fabricated Cu/Pd grating structures by μ-molding in capillaries (MIMIC) and electroless deposition technique (Figure 2). First, thin Pd seed lines were obtained by a single step MIMIC process developed in the laboratory.[38] In brief, the Pd hexylthiolate precursor (1 mM) was thermolyzed at 250 °C for 1 h inside the capillary channels of a PDMS mold. The Pd grating lines (~10 nm thick) fabricated on the glass substrate are ~1 μm wide with a spacing of ~500 nm and extend uniformly over large areas. The grating is transmitting up to 85% but as such not so well conducting (> MΩ/sq). To improve the value of sheet resistance without sacrificing much in transmittance, Cu was brought over Pd by the electroless deposition method[39] as shown in the schematic

dx.doi.org/10.1021/am302264a | ACS Appl. Mater. Interfaces 2013, 5, 730−736

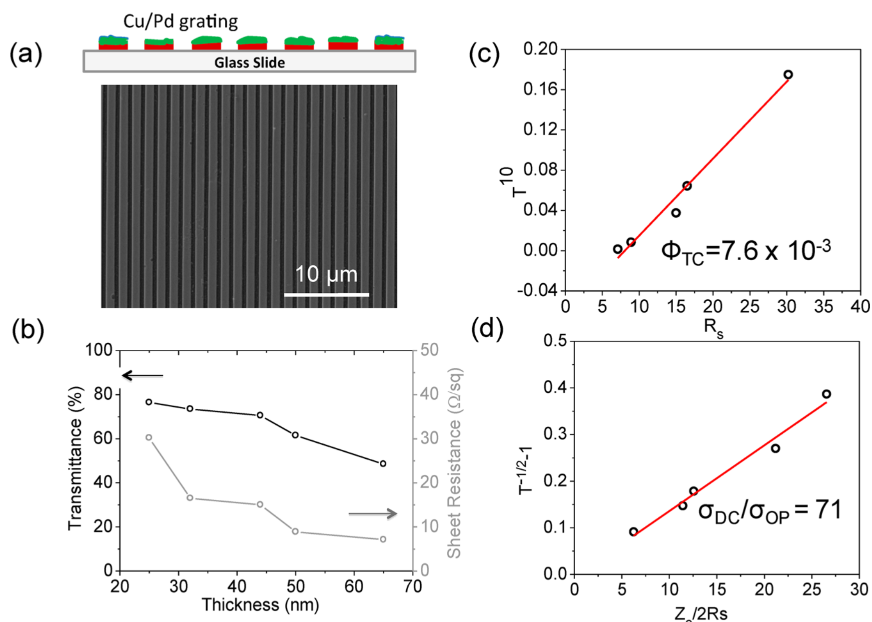

Figure 2. (a) FESEM image of a Cu/Pd grating with schematic on top. (b) Variation in average transmittance and sheet resistance versus thickness of Cu on Pd grating. Transmittance (T) and sheet resistance (R_S) expressed using equations $\phi_{TCE} = T^{10}/R_S$ and $T = (1 + z_o\sigma_{OP}/2R_S\sigma_{DC})^{-2}$ in plots (c) and (d), respectively.

in Figure 2a (detailed in SI Figure S1); Cu being less expensive, is preferred.

The grating structures with different thicknesses of Cu on Pd were obtained by optimizing the electroless plating time conditions (Figure S2). The transmittance and I−V characteristics of the different Cu/Pd μ-MGPs were obtained as shown in Figure S3. The transmittance curves are flat and essentially featureless in the visible spectral range (400−800 nm). Once Cu was deposited on the Pd seed layer, the sheet resistance decreased from several MΩ to 30 Ω/sq, for which the transmittance was ∼78%. Microscopic analysis has shown that Cu essentially filled voids in Pd seed layer and increased the average thickness to 25 nm from the initial 10 nm (see Figure S4). The resistance could be further lowered to 6 Ω/sq by depositing ∼55 nm thick Cu, but with a compromise on transmittance (∼ 48%, see Figure 2b). The Cu/Pd μ-MGPs with transmittance above 70% and sheet resistance between 15 and 30 Ω/sq may be considered good for TCE-based applications. The Figure of Merit (FoM) values were calculated directly from the slope of plots in Figure 2b. The ϕ_{TCE} calculated using eq 1 works out to be 7.6 × 10^{-3} (Figure 2c) which is close to that of commercial ITO. The FoM based on σ_{DC}/σ_{OP} is ∼71 as seen in Figure 2d. This value may be compared with the best values reported for CNT films (typically between 10 and 25)[40] and graphene-based TCEs (1−15).[26] A σ_{DC}/σ_{OP} value of 500 has been reported for Ag nanowire networks.[22] The FoM values of TCEs sourced from literature are tabulated in Table S2.

Unlike the case of network structures, the patterned Cu/Pd μ-MGPs can be easily pixelized which goes in sync with display applications where pixelization is ubiquitous. Being periodic, it can be a diffraction grating too. The diffraction is particularly useful in increasing the absorption for photovoltaic applications[41] whereas for display applications, the grating parameters are to be formulated considering the diffraction limit.[34] A laser beam (λ = 650 nm) collimated to a diameter of ∼500 μm was made incident on the Cu/Pd μ-MGPs covering the whole pixel area. The laser beam gets diffracted at an angle of 25.8° (calculated using the grating equation, $d{\cdot}\sin\theta = \eta\lambda$) in the

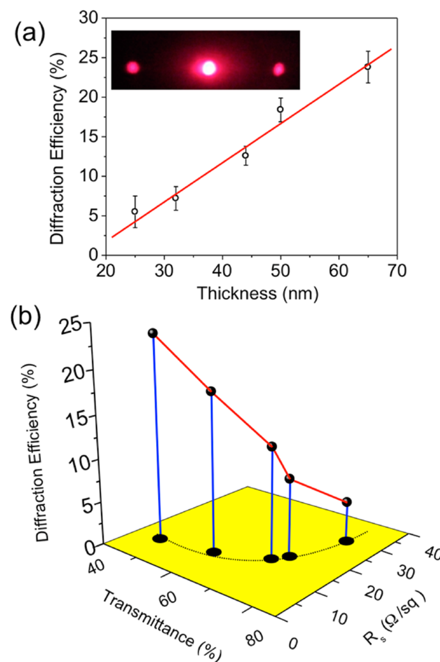

Figure 3. (a) Diffraction efficiency versus thickness of the grating with inset showing a photograph of typical diffraction pattern. The intensity profile is shown overlaid. (b) 3D plot demonstrating the diffraction efficiency dependence on sheet resistance and transmittance.

transmission geometry. The diffraction efficiency, DE (ratio of first order and zeroth order spot intensities), is known to be proportional to the thickness of grating. The mathematical relation that relates DE to the grating thickness (t) is given as[42]

$$DE = \left(\frac{\pi t}{\lambda \cos\theta}\right)\left\{\exp\left[\frac{-2.303OD(\lambda)}{\cos\theta}\right]\right\}((\Delta\eta^2 + \Delta\kappa^2)) \quad (2)$$

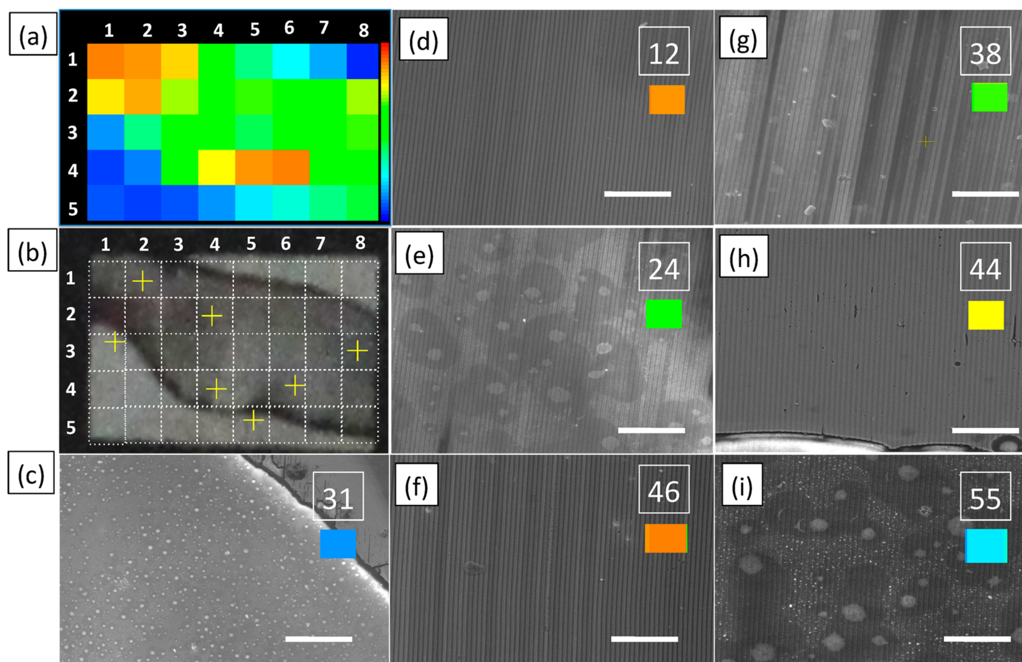

Figure 4. (a) Diffraction efficiency mapping of the Cu/Pd patterned grating over a 4 mm × 2.5 mm area with each pixel of 0.5 mm × 0.5 mm (z-scale: 0−7, 50 hues). The row and column numbers are indicated along top and left edges to specify position of each pixel. (b) Optical photograph of the patterned area with white dotted lines indicating the pixels over which the diffraction efficiency map is obtained. The plus sign marked in different pixels indicate zoomed-in SEM images (c)−(i) (scale bar, 20 μm). In each case, the center of the plus sign is the center of the image. The pixel number is indicated at the top right corner. The color bar shows the variation in DE between 0 and 7 with different color levels as visual indicators of the local variations on the sample surface.

Indeed, the DE value increased linearly with the thickness of Cu deposited on Pd, as shown in Figure 3a. Its dependence on R_S and T can be clearly seen from the 3D plot shown in Figure 3b. The higher DE is associated with lower T and R_S whereas DE decreases as the T and R_S increase. This clearly shows that the diffraction efficiency is intimately linked to T and R_S.

Apart from the grating thickness, optical properties of the grating, namely the modulations in real and imaginary part of refractive index, $\Delta\eta$ and $\Delta\kappa$ respectively, and the optical density at the given wavelength, $OD(\lambda)$, can influence DE. In fact, any variation in DE from the probed region (pixel), should point to variation in one or more of these parameters and thus DE is projected as a supervisor parameter or LFoM. Specifically, in the case of Cu/Pd μ-MGPs, sheet resistance can be written as $R_S = 1/\sigma_{DC} \cdot t \cdot f$, where f is the fill factor of the grating in relation to a uniform film and σ_{DC} is DC conductivity. Therefore, the variation in R_s depends on the local values of f and t. Substituting, $t = 1/\sigma_{DC} \cdot R_S \cdot f$ and $OD(\lambda) = -\log T(\lambda)$, ($T(\lambda)$ being transmittance) in eq 2 and rearranging the terms, we get the following.

$$DE_{pixel} = \left(\frac{T}{R_S}\right) \times \left\{\left(\frac{1}{f \cdot \cos\theta}\right) e^{1/\cos\theta}(\Delta\eta^2 + \Delta\kappa^2)\right\} \times \left(\frac{\pi}{\lambda \cdot \sigma_{DC}}\right) \tag{3}$$

The first term, T/R_S, is effectively FoM of the pixel typically of the beam size. The second term with parameters f, θ, $\Delta\eta$, and $\Delta\kappa$ stand for local variations, while the third term has all the constants. Thus, eq 3 may be rewritten as $DE_{pixel} = FoM_{pixel} \times$ *local parameters* $\times$ *constant* = LFoM.

As diffraction can be obtained over every pixel, the DE value obtained can be used to locally monitor the quality of the TCE. While the scattering due to defects adversely affects the zeroth order intensity, local variations in the periodicity of the grating structure diminish the first order intensity. The morphological differences and defects mentioned in Figure 1 are in a way stored in the DE value which is sensitive down to the third decimal place.[43]

For illustration, DE values from a standard transmission grating were collected encompassing disordered regions as well (see Figure S5) by rastering the laser beam across the pixelized (imaginary) grating using a translation stage (Figure S6). The DE values were noticeably lower in defective areas. The quality of a given area of TCE can be examined by collecting the diffraction data from its every pixel in the form of a DE map. In Figure 4a is shown a DE map generated for a 4 mm × 2.5 mm area on a Cu (25 nm)/Pd (10 nm) μ-MGP for pixel size of 0.5 mm × 0.5 mm. The corresponding optical photograph, with the imaginary pixels marked, is shown in Figure 4b. For the purpose of illustration, the mapped area was chosen such that the area contained regions of varied quality of the grating and also extended well beyond the molded region. The molded region is seen darker in transmission compared to the outside regions on either side, which contained some debris from the fabrication process. The DE values are seen to vary depending on the quality of grating pattern, with a high value of $DE \approx 6$ (seen as red in Figure 4a) corresponding to a better quality pattern. The DE landscape can be correlated with the nature of the grating structure using FESEM images shown in Figure 4c−i, from the different pixels. In pixel 31, only a small fraction of the area is the patterned grating and therefore this pixel has a low DE value, 0.467 (Figure 4c). This is also true of pixels 41, 51, 18 etc. (images not shown). The other marked pixels 12, 24, 38, 44, and 46 all lie inside the patterned area exhibiting DE values of 5.991, 5.262, 4.594, 3.462, and 4.383 respectively, whereas pixel 55 with a DE of 1.518 is closer to the edge.

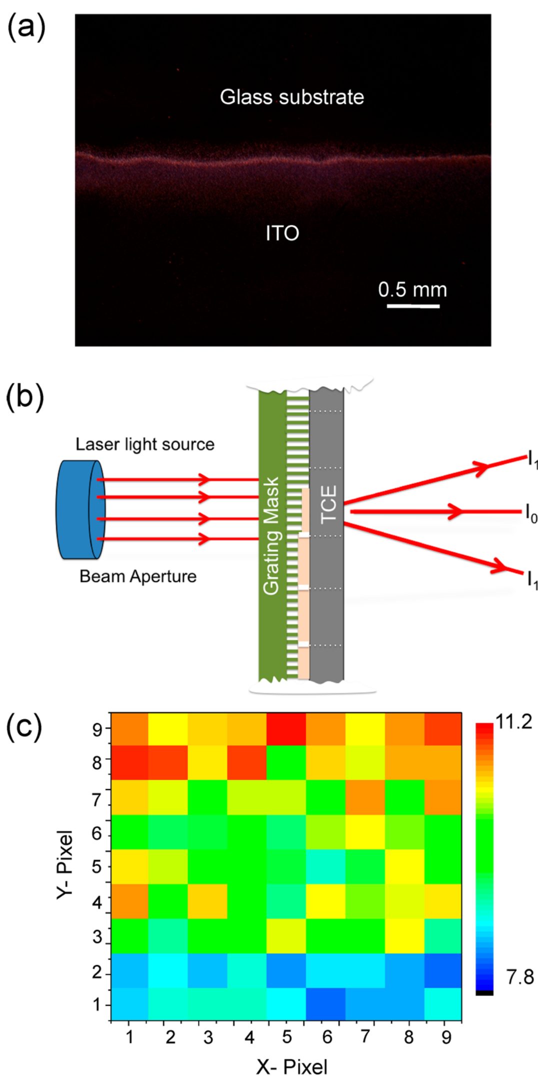

Figure 5. (a) Dark field microscope image of the interface of etched ITO on glass substrate. (b) Schematic of the diffraction setup with ITO containing an etched step. (c) Diffraction efficiency map of 4.5 mm × 4.5 mm for grating mask sandwiched to the ITO glass surface. Each pixel measures 0.5 mm × 0.5 mm.

From the images in Figure 4d–i, the pixels 12 and 46 indeed appear better in terms of grating structure than the pixel 44, which carried some major defects at the bottom and, therefore, has a lower *DE* value. The variations in *DE* values from pixel to pixel are truly representative of the microscopic structure/defects within the pixels.

Not all TCEs are grating structures, it is the other way mostly. To extend this method to nongrating structured TCEs such as an ITO substrate, an external grating was overlaid on it to enable diffraction. Light diffracted through a calibrated transparent grating coupled with a nonperiodic TCE is also structured carrying geometry and material specific information, as if it is an extended grating (see Figure 1b, right). In this case, the variations due to defects in the TCE are expected to influence $\Delta\eta$ and $\Delta\kappa$ of the "extended" grating as illustrated by taking examples of different defect-containing regions marked 1–6 in Figure 1b.

Therefore, the *DE* value obtained may well be used for monitoring the quality of a TCE. For the sake of illustration, a step profile was created on a ITO coated glass (thickness of 120 nm) by etch stripping a small region with Zn/HCl, as is usually done during device fabrication.[44] To evaluate the quality of the ITO film, the substrate was overlaid with a grating structure derived from a CD (grating period, ~1.5 μm) and the *DE* map was obtained over a 4.5 mm × 4.5 mm area in a 9 × 9 pixel grid covering the step (see schematic in Figure 5b). By comparing Figure 5a and c, we see that while the dark field image demarcates the stepped region, the *DE* map brings out the thickness variations across the step. The pixels corresponding to glass only region exhibit higher *DE* values (~ 10, equal to the original *DE* from the grating), while *DE* values are somewhat lower (~ 8) from pixels on ITO, as there would be some scattering and other nonuniformities.

Polyethylene terephthalate (PET) is being increasingly projected as a flexible substrate for TCEs. In comparison to the conventional glass substrate, ITO on PET tends to develop cracks during transport, fabrication, and use.[45] In the experiment described below (Figure 6), we have compared the *DE* maps of two as-supplied ITO films, one on PET (80 ± 5 nm) and another on glass (120 ± 2 nm) substrate. The total area and the pixel size were kept the same in both the cases. Without ITO, both PET and glass have negligible influence on the *DE* value of the overlaid grating, which is typically above 9.0. ITO coating brings down the *DE* value to some extent. In case of ITO on glass (Figure 6a), the pixels in the *DE* map are uniformly greenish except a few pixels which are blue and red. The mean value of *DE* is 7.734% with a standard deviation of 0.376%. On the other hand, the average *DE* value for ITO on PET was estimated to be 7.914 ± 1.036%. The higher value of the mean in the latter is due to lesser thickness of the ITO film

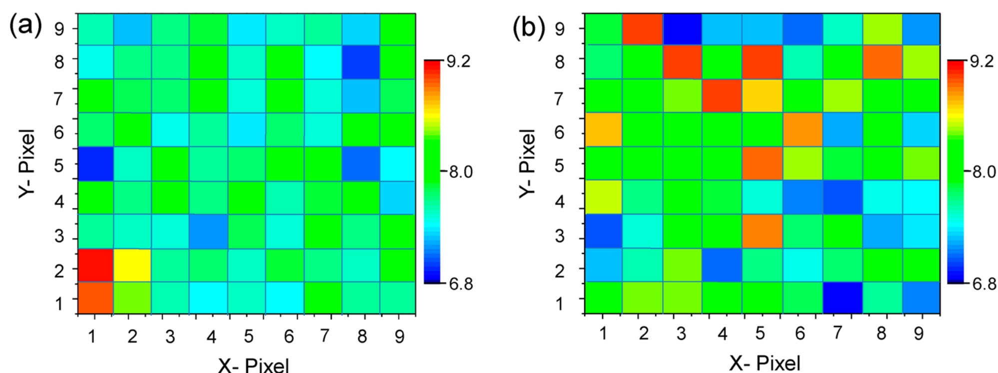

Figure 6. Diffraction efficiency maps from 4.5 mm × 4.5 mm grating overlaid with (a) ITO on glass and (b) ITO on PET sheet measured. Each pixel measures 0.5 mm × 0.5 mm.

dx.doi.org/10.1021/am302264a | ACS Appl. Mater. Interfaces 2013, 5, 730–736

($\Delta t \approx 40$ nm). Interestingly, the standard deviation in the mean value is also higher (many blue and red pixels all over, see Figure 6b) indicating higher disorder or nonuniformity in the ITO film coated on PET. Such nonuniformity may have detrimental effect on the efficiency of the device in use,[46] which can not be singled out while pixelwise testing.[47] It is important to perform screening prior to device fabrication to save material cost and effort.

TCEs by definition, are highly transmitting and are not amenable for visual or photographic inspection. Even if one does, it may not be quantitative enough. Often, the scattering of light from defects in a transmitting medium does not produce enough contrast for easy identification. It is for the same reason and also because of the focusing errors, that techniques such as optical profilometry are not always suitable especially for inspection of large areas of highly transmitting sheets.[48] Moreover, microscopy-based techniques suffer from diffraction-limited resolution, which is typically ~1 μm. This underlines the importance of a sensitive technique such as optical diffraction, which can detect sub-μm spatial variations in the Fourier space as demonstrated in this article. While we have used a sizable beam diameter to scan sub-mm pixels (relevant in large area displays), the method is not necessarily restrictive. One may develop an automated scanning setup with both beam diameter and pixel size within a few μms. This work is currently under progress.

■ CONCLUSIONS

The present study brings out the significance of defining a local figure of merit (LFoM) for TCEs, in addition to the general figure of merit assigned as a measure of the overall quality of the TCEs. As the presence of nonuniformity and defects in pixels can seriously hamper functioning of a TCE, the LFoM should pertain to individual pixels. Accordingly, a method based on measuring diffraction efficiency of a micrometer periodicity transmission grating coupled with TCE was developed and applied to a few case examples (ITO/glass and ITO/PET). The *DE* values from pixels depicted in the form of a map could be readily correlated with the nonuniformities and defects as examined qualitatively by microscopy. The standard deviation in *DE* value was observed to be 0.4% for the ITO/glass and 1% for ITO/PET. The *DE* map is thus a quantitative measure of the nonuniformities, with high sensitivity.

As an example of new-generation TCE, a metal grating pattern of Cu/Pd μ-MGPs with transmittance above 70% and sheet resistance between 15 and 30 Ω/sq was fabricated by depositing a Pd seed layer following micromolding and bringing Cu on top by electroless deposition. The value of σ_{DC}/σ_{OP} as figure of merit was calculated to be 71, and ϕ_{TCE} was 7.6×10^{-3}. To further emphasize the importance of local FoM, it was locally examined by mapping of *DE* and we could distinguish the varying qualities of different regions by relating to the high-resolution microscopy images. The *DE* mapping technique will have greater implications in the case of nanostructured based emerging TCEs. An automated data collection should enable fast screening of large areas.

■ EXPERIMENTAL SECTION

Micrograting Pattern of Cu Deposited on Pd. The process of fabrication of Pd seed layer is illustrated in Supporting Information Figure S1a. The precursor, Pd hexadecylthiolate, $Pd(SC_{16}H_{33})_2$, in toluene was synthesized following the method reported previously.[38] The synthesis of precursor involves a single-step procedure. Pd acetate (5.0 mmol) in 7 mL of toluene was added to 5.0 mmol hexadecylthiol in toluene (3 mL), and the resulting mixture was stirred vigorously overnight resulting in a yellow solution which was diluted to obtain a toluene solution of 1 mM concentration. The copper plating bath used for electroless Cu deposition consisted of solution A (1.5 g of $CuSO_4$, 7 g of $KNaC_4H_4O_6 \cdot 4H_2O$, and 7 g of NaOH in 50 mL of water) and solution B (37.2 wt % aqueous formaldehyde solution). The two solutions were taken in 10:1 (v/v) ratio and mixed together just before the electroless plating was performed. Each substrate was taken out after a predetermined time interval and immersed in a water bath to arrest the reaction. The substrates were vacuum-dried prior to diffraction experiments.

Diffraction Measurements. These were performed using a diode laser source (650 nm, 3 mW) focused normal to the grating surface mounted on an X-Y-Z translation stage (Thorlabs MAX313/M). The transmitted light after diffraction was measured using a photodiode (Thorlabs, DET 200) connected to digital oscilloscope (Hewlett-Packard-54600B, 100 MHz). The intensity of diffraction spots was measured from a fixed distance (3 cm) from the sample by placing the photodetector adjacent to screen position. In the case of nonperiodic structures, such as ITO film, an external grating was used. The transmission grating used in these experiments was simply a small portion of (1 cm × 1 cm) of a commercially available compact disk (Sony CD-R) obtained after peeling off the Al encapsulation and washing away the dye layer. The grating thus prepared contained grating lines of 1.5 μm periodicity and height of ~180 nm. The laser beam was made to transmit through the ITO film overlaid with the CD grating using mechanical clips. The diffraction spots were photographed using a digital camera. AFM measurements were performed using di Innova SPM (Veeco, USA) in the tapping mode. Standard Si cantilevers (model RTSPA) were used for the normal topography imaging. The patterned substrates were also examined under a Nova NanoSEM 600 instrument (FEI Co., The Netherlands). Energy-dispersive spectroscopy (EDS) analysis was performed with an EDAX Genesis instrument (Mahwah, NJ) attached to the SEM column. UV−visible spectra were recorded using a Perkin−Elmer Lambda 900 UV/visible/near-IR spectrophotometer. The film thickness measurements were done using a stylus profilometer (Dektek 6M, Veeco). For resistance measurements, physical vapor deposition of Au was carried out on a shadow mask using a thermal evaporator (Hind Hivac, India) at a base pressure of 10^{-6} Torr. Current−voltage measurements were done using a Keithley 236 source measure unit. The dark field image was captured using a microscope from Laben Instruments, India IM-20BD, equipped with a darkfield condensor and a CCD camera (Pixel Link, PL-S621CU).

■ ASSOCIATED CONTENT

Supporting Information

Table for different definitions of Figure of Merit for TCE proposed in literature, the schematic of the process involved in the fabrication of Cu/Pd along with microscopy, calibration curve for electroless deposition time and thickness, transmission spectra and I−V characterstics of Cu/Pd μ-MGPs, tabulated values for Figure of Merit sourced from literature, setup for diffraction mapping. This material is available free of charge via the Internet at http://pubs.acs.org.

■ AUTHOR INFORMATION

Corresponding Author

*E-mail: kulkarni@jncasr.ac.in. Phone: +91(80) 22082814. Fax: +91 (80) 22082766.

Notes

The authors declare no competing financial interest.

■ ACKNOWLEDGMENTS

The authors thank Professor C. N. R. Rao, FRS for his support and encouragement. The financial support from DST, India for EU-Indian framework of the Large Cells project is gratefully

acknowledged. Funding source: Department of Science and Technology, Government of India. The manuscript was written through contributions of all authors. All authors have given approval to the final version of the manuscript.

■ ABBREVIATIONS

ITO = indium−tin-oxide
PET = polyethylene terephthalate
μ-MGPs = μ-metal grating patterns
CD = compact disc
MIMIC = μ-molding in capillaries
OD = optical density
PDMS = polydimethyl siloxane
TCE = transparent conducting electrode
FoM = Figure of Merit
DE = diffraction efficiency

■ REFERENCES

(1) Hecht, D. S.; Hu, L.; Irvin, G. *Adv. Mater.* **2011**, *23*, 1482.
(2) Pasquarelli, R. M.; Ginley, D. S.; O'Hayre, R. *Chem. Soc. Rev.* **2011**, *40*, 5406−5441.
(3) Ellmer, K. *Nat. Photonics* **2012**, *6*, 809−817.
(4) De, S.; King, P. J.; Lotya, M.; O'Neill, A.; Doherty, E. M.; Hernandez, Y.; Duesberg, G. S.; Coleman, J. N. *Small* **2010**, *6*, 458−464.
(5) Becerril, H. A.; Mao, J.; Liu, Z.; Stoltenberg, R. M.; Bao, Z.; Chen, Y. *ACS Nano* **2008**, *2*, 463−470.
(6) Eda, G.; Fanchini, G.; Chhowalla, M. *Nat. Nanotechnol.* **2008**, *3*, 270.
(7) Wassei, J. K.; Kaner, R. B. *Mater. Today* **2010**, *13*, 52−59.
(8) Lotya, M.; Hernandez, Y.; King, P. J.; Smith, R. J.; Nicolosi, V.; Karlsson, L. S.; Blighe, F. M.; De, S.; Wang, Z.; McGovern, I. T.; et al. *J. Am. Chem. Soc.* **2009**, *131*, 3611.
(9) Tung, V. C.; Allen, M. J.; Yang, Y.; Kaner, R. B. *Nat. Nanotechnol.* **2009**, *4*, 25.
(10) Wang, X.; Zhi, L.; Mullen, K. *Nano Lett.* **2007**, *8*, 323.
(11) Dan, B.; Irvin, G. C.; Pasquali, M. *ACS Nano* **2009**, *3*, 835.
(12) Nasibulin, A. G.; Kaskela, A.; Mustonen, K.; Anisimov, A. S.; Ruiz, V.; Kivistö, S.; Rackauskas, S.; Timmermans, M. Y.; Pudas, M.; Aitchison, B.; Kauppinen, M.; Brown, D. P.; Okhotnikov, O. G.; Kauppinen, E. I. *ACS Nano* **2011**, *5*, 3214.
(13) Rowell, M. W.; Topinka, M. A.; McGehee, M. D.; Prall, H. J.; Dennler, G.; Sariciftci, N. S.; Hu, L.; Gruner, G. *Appl. Phys. Lett.* **2006**, *88*, 233506.
(14) Wang, R.; Sun, J.; Gao, L.; Zhang, J. *ACS Nano* **2010**, *4*, 4890.
(15) Wu, Z.; Chen, Z.; Du, X.; Logan, J. M.; Sippel, J.; Nikolou, M.; Kamaras, K.; Reynolds, J. R.; Tanner, D. B.; Hebard, A. F.; Rinzler, A. G. *Science* **2004**, *305*, 1273.
(16) Lee, J. Y.; Lee, J.-Y.; Connor, S. T.; Cui, Y.; Peumans, P. *Nano Lett.* **2008**, *8*, 689.
(17) Yang, L.; Zhang, T.; Zhou, H.; Price, S. C. B.; Wiley, J.; You, W. *ACS Appl. Mater. Interfaces* **2011**, *3*, 4075−4084.
(18) Rathmell, A. R.; Bergin, S. M.; Hua, Y.-L.; Li, Z.-Y.; Wiley, B. J. *Adv. Mater.* **2010**, *22*, 3558.
(19) Wu, H.; Hu, L.; Rowell, M. W.; Kong, D.; Cha, J. J.; McDonough, J. R.; Zhu, J.; Yang, Y.; McGehee, M. D.; Cui, Y. *Nano Lett.* **2010**, *10*, 4242.
(20) De, S.; Higgins, T. M.; Lyons, P. E.; Doherty, E. M.; Nirmalraj, P. N.; Blau, W. J.; Boland, J. J.; Coleman, J. N. *ACS Nano* **2009**, *3*, 1767.
(21) King, P. J.; Khan, U.; Lotya, M.; De, S.; Coleman, J. N. *ACS Nano* **2010**, *4*, 4238.
(22) Zeng, X.-Y.; Zhang, Q.-K.; Yu, R.-M.; Lu, C.-Z. *Adv. Mater.* **2010**, *22*, 4484.
(23) Shim, B. S.; Zhu, J.; Jan, E.; Critchley, K.; Kotov, N. A. *ACS Nano* **2010**, *4*, 3725.
(24) De, S.; King, P. J.; Lyons, P. E.; Khan, U.; Coleman, J. N. *ACS Nano* **2010**, *4*, 7064.
(25) Haacke, G. *J. Appl. Phys.* **1976**, *47*, 4086.
(26) De, S.; Coleman, J. N. *ACS Nano* **2010**, *4*, 2713.
(27) Barnes, T. M.; Reese, M. O.; Bergeson, J. D.; Larsen, B. A.; Blackburn, J. L.; Beard, M. C.; Bult, J.; van de Lagemaat, J. *Adv. Energy Mater.* **2012**, *2*, 353−360.
(28) Kaskela, A.; Nasibulin, A. G.; Timmermans, M. Y.; Aitchison, B.; Papadimitratos, A.; Tian, Y.; Zhu, Z.; Jiang, H.; Brown, D. P.; Zakhidov, A.; Kauppinen, E. I. *Nano Lett.* **2010**, *10*, 4349.
(29) Doherty, E. M.; De, S.; Lyons, P. E.; Shmeliov, A.; Nirmalraj, P. N.; Scardaci, V.; Joimel, J.; Blau, W. J.; Boland, J. J.; Coleman, J. N. *Carbon* **2009**, *47*, 2466.
(30) De, S.; Lyons, P. E.; Sorel, S.; Doherty, E. M.; King, P. J.; Blau, W. J.; Nirmalraj, P. N.; Boland, J. J.; Scardaci, V.; Joimel, J.; Coleman, J. N. *ACS Nano* **2009**, *3*, 714.
(31) Hecht, D. S.; Thomas, D.; Hu, L.; Ladous, C.; Lam, T.; Park, Y.; Irvin, G.; Drzaic, P. *J. Soc. Inf. Display* **2009**, *17*, 941.
(32) Wang, J.; Liang, M.; Fang, Y.; Qiu, T.; Zhang, J.; Zhi, L. *Adv. Mater.* **2012**, *24*, 2874−2878.
(33) Lee, S.; Lee, K.; Liu, C. H.; Zhong, Z. *Nanoscale* **2012**, *4*, 639.
(34) Catrysse, P. B.; Fan, S. *Nano Lett.* **2010**, *10*, 2944.
(35) Tvingstedt, K.; Inganäs, O. *Adv. Mater.* **2007**, *19*, 2893.
(36) Kang, M. G.; Guo, L. J. *Adv. Mater.* **2007**, *19*, 1391.
(37) Kang, M. G.; Kim, M. S.; Kim, J.; Guo, L. J. *Adv. Mater.* **2008**, *20*, 4408.
(38) Boya, R.; Sagade, A. A.; Gupta, R.; Kulkarni, G. U. *J. Nanosci. Nanotechnol.* **2011**, *11*, 152.
(39) Hidber, P. C.; Helbig, W.; Kim, E.; Whitesides, G. M. *Langmuir* **1996**, *12*, 1375−1380.
(40) Madaria, A. R.; Kumar, A.; Zhou, C. *Nanotechnology* **2011**, *22*, 245201.
(41) Dewan, R.; Knippa, D. *J. Appl. Phys.* **2009**, *106*, 074901.
(42) Shallcross, R. C.; Chawla, G. S.; Marikkar, F. S.; Tolbert, S.; Pyun, J.; Armstrong, N. R. *ACS Nano* **2009**, *3*, 3629−3637.
(43) Lu, P. P. PhD. Dissertation, Diffraction gratings for optical sensing, Stanford University, September 2009.
(44) Chen, M. F.; Chen, Y. P.; Hsiao, W. T.; Gu, Z. P. *Thin Film Solids* **2007**, *515*, 8515−8518.
(45) Cotterell, B.; Chen, Z. *Int. J. Fract.* **2000**, *104*, 169−179.
(46) Bhagat, S. K.; Han, H.; Zoo, Y.; Lewis, J.; Grego, S.; Lee, K.; Iyer, S.; Alford, T. L. *Thin Solid Films* **2008**, *516*, 4064−4069.
(47) Krebs, F. C.; Søndergaard, R.; Jørgensen, M. *Sol. Energy Mater. Sol. Cells* **2011**, *95*, 1348−1353.
(48) Visscher, M.; Struik, K. G. *Prec. Eng.* **1994**, *16*, 192−98.